Available online at www.sciencedirect.com
SCIENCE DIRECT®
Journal of Nuclear Materials 337–339 (2005) 1015–1018
journal of nuclear materials
www.elsevier.com/locate/jnucmat

# Incident-mass dependence of temperature-enhanced ion-induced sputtering in liquid metals

M.D. Coventry *, D.N. Ruzic

*Department of Nuclear, Plasma, and Radiological Engineering, University of Illinois at Urbana-Champaign, 103 S. Goodwin Ave., Urbana, IL 61801, USA*

**Abstract**

The sputtering yield of liquid tin due to heavy-ion bombardment has been found to have significantly reduced dependence on the sample temperature than that of light-ion bombardment. These results, combined with previous light-ion data, show that the mechanisms that increase the sputtering yield of materials under ion irradiation are diminished or surpassed by the effects of heavy-ion bombardment. Beams of 700 eV $Ne^+$ and 500–1000 eV $Ar^+$ ions irradiated high-purity tin at temperatures from 20–340 °C at oblique incidence; a pair of quartz–crystal microbalances performed real-time measurement of the mass ejected from the surface. Monte Carlo atomistic simulations were also performed for comparison and to help interpret the experimental results. We discuss the results of this series of experiments and the lack of a comprehensive understanding of the mechanisms behind temperature-dependent sputtering in light of these results.


*PACS:* 79.20.R; 28.52.F; 34.50.D
*Keywords:* Ion-surface interactions; Sputtering; Divertor material; Liquid metal; Erosion; Deposition

## 1. Introduction

Liquid tin is one of several molten metals in consideration for use as a plasma-facing component (PFC) in future, high power, high duty cycle magnetic fusion machines [1]. A good understanding of the response of a liquid tin surface during ion irradiation is necessary to model the divertor region correctly, whose plasma is tightly coupled with the edge plasma and can strongly influence the core plasma. Also important is an understanding of any changes in these responses due to elevated surface temperatures as such a divertor will be operated at high temperatures, particularly on a transient basis. Similar to that of other liquid metal PFC candidates [2–5], tin's sputtering yield due to low-energy, light ion bombardment exhibits clear temperature dependence [6,7].

The purpose of this series of experiments was to examine how this temperature dependence scales with incident particle mass for the specific case of liquid tin. Fig. 1 shows previously-reported [6] light-ion data for comparison. While $D^+$, $He^+$, and $Sn^+$ are clearly the most useful incident ions to have sputtering yield information for a divertor design study, intermediate masses were used here to examine any scaling of the temperature dependence of the sputtering yields on incident

* Corresponding author. Tel.: +1 217 333 6291; fax: +1 217 333 2906.
*E-mail address:* coventry@uiuc.edu (M.D. Coventry).

0022-3115/$ - see front matter © 2004 Elsevier B.V. All rights reserved.
doi:10.1016/j.jnucmat.2004.10.088

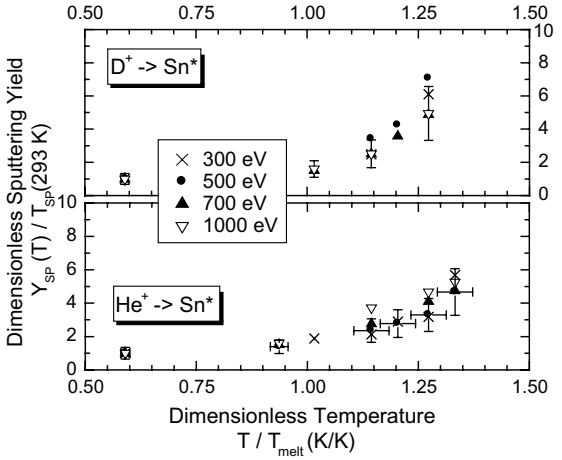


Fig. 1. This figure presents previous results showing presence of temperature-enhancement of the sputtering yield of light-ion bombardment for of tin at 45° incidence. Even in these results, clear differences can be seen by changing the bombarding ion species. The VFTRIM simulation results for both of these cases closely match the solid tin data and are not shown in this figure; however, VFTRIM cannot, at present, to model sample temperature changes.

mass. With previous $D^+$ and $He^+$ sputtering data [6], the data reported here, and future tin self-sputtering data (our next series of experiments), target-to-incident particle mass ratios from 60 to unity will be covered, with 30, 6, 3 spanning the gap. While this sputtering data may not be directly usable in a divertor design study, the understanding of the dependencies of temperature enhanced sputtering will allow estimation of other untested systems and allow for clearer extrapolation.

A rigorous model of the physical mechanism behind the temperature enhancement has yet to be developed. However, two preliminary models [8,9] make attempts at understanding the underlying processes. Neither, however, have an explanation for the discrepancy of the heavy-ion results with those of light ions.

## 2. Experimentation and data analysis

The facility used for this series of experiments was the ion-surface interaction experiment (IIAX) [10,11]. IIAX uses a differentially-pumped G-1 Colutron [12] ion source with an array of ion optics and filters to provide a velocity-filtered, low-energy ion beam – currently at a 45° angle of incidence from the surface normal – to bombard the selected target. The target sample and its heater are electrically isolated from each other and from earthground to allow direct monitoring of the beam current. Separate experiments determined the ion-induced electron emission coefficient. For neon and argon, ion currents on the order of hundreds of nanoamperes and beam spot sizes around $10^{-5}m^2$, fluxes of $10^{13}$ ions/$m^2$s are reached. Typically, the total fluence on target reaches $10^{20}$ ions/$m^2$.

The sample itself is a 1.0 mm thick, 12 mm diameter disk held vertically by a stainless steel backing plate/retainer ring and a tantalum retention shield; the retention shield has a 3.5 mm aperture through which the liquid sample is irradiated. A thermocouple is spot-welded directly to the retention shield to closely monitor the sample temperature. The standard UHV substrate heater has recently been used at partial power levels 100% of the time instead of full power part of the time; although this takes additional time to equilibrate and calibrate in comparison, it reduces thermal cycling-induced diagnostic-signal oscillations.

A quartz–crystal microbalance (QCM) collects and measures a fraction, typically 10–20%, of the material sputtered from the target by the ion beam. A second QCM, that sees very little (<0.01%) sputtered material, is used to monitor background effects, which are then removed from the foreground signal. Such background effects include laboratory temperature variations influencing the oscillation circuits and mechanical vibrations in the manipulator-mounted QCM head. Fig. 2 shows a depiction of the IIAX target chamber and the relative placement of this key diagnostic.

From that the mass of material deposited, the rate of tin particles deposited can be determined, provided the deposited film stoichiometry. For heavy-ion tin sputtering, we assume that the deposited surface is pure tin, based on the fact that tin oxidizes slowly and the tin flux to the crystal is an order of magnitude greater than the flux from the ambient oxygen at a partial pressure near $10^{-7}$ Pa. However, the sticking coefficient of sputtered tin on the tin-covered crystal is not unity, and therefore must be taken into consideration. The sticking coefficient of tin particles on tin was measured by Fontell and Arminen [13] over a wide range of energies including those of typical sputtered particles; values from this work were used for data analysis. This calculation tells us the rate of tin particle bombardment on the crystal surface. The remaining factor that plays a major role in determining the sputtering yield from crystal deposition data is the fraction of material ejected that actually strikes the crystal. This geometric factor is determined by the distribution pattern of the ejected particles that we assume scales with the cosine of the polar angle from the surface normal and is independent of the azimuthal angle. From this, and known system geometry, we perform a surface integration over the crystal face and use the ratio of that to the surface integral over $2\pi$ steradians (due to the weighting, the total weighted solid angle is steradians for a polar angle ranging from 0 to $\pi/2$). Finally, we perform a minor correction for the material that initially sticks on the crystal surface, but

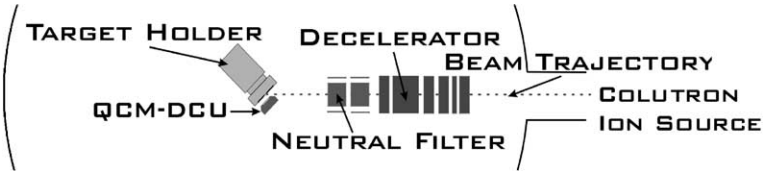


Fig. 2. This depiction of the ion–surface interaction experiment (IIAX) target chamber is from a bird's eye view. The background crystal is found 30 mm directly above the foreground crystal. Not shown is the Colutron [12] ion source providing the low-energy beam from the right.

is then sputtered off by ions reflecting off of the sample. This involves the product of the geometric factor, which is the same as that for the sputtered material $f_{geo}$; the reflection coefficient of the incident ions from the sample, $R_{inc}$; and the sputtering yield of the reflected ions onto the tin-covered crystal, $Y_{ref}$. Both $R_{inc}$ and $Y_{ref}$ are determined using VFTRIM [14], a variant of the TRIM.SP [15] sputtering simulation code. The simulation used to determine the reflection coefficient also produces an average reflected particle energy, which is used to determine the sputtering yield of the reflected ions. While molecular dynamic simulation or empirical measurement of these processes would be more accurate, obtaining a reliable interaction potential for the surface atoms is challenging and the availability of such data is limited.

In summary, starting with the frequency data and the directly measured ion current, the following equation is used to determine the absolute sputtering yield:

$$Y = \frac{K \cdot \langle \delta_{net} \rangle}{M \cdot SC \cdot f_{geo} \cdot \langle I \rangle} + f_{geo} \cdot R_{inc} \cdot Y_{ref}, \quad (1)$$

where $K$ is a constant for a given initial frequency and type of crystal that converts the rate of frequency change into a rate of mass change; $\langle \delta_{net} \rangle$ is the mean difference of the time derivatives of the foreground and background crystal frequencies; $M$ is the mass deposited per tin particle; $SC$ is the sticking coefficient of the sputtered material on a tin-covered crystal; $f_{geo}$ is the fraction of material ejected that strikes the crystal due to system geometry; and $\langle I \rangle$ is the mean ion current compensated for ion-induced electron emission.. Values of these terms used for analysis of these data are presented in Table 1.

Table 1
These parameter values were used during data analysis

| | 700 eV $Ne^+$ | 500 eV $Ar^+$ | 700 eV $Ar^+$ | 1000 eV $Ar^+$ |
|---|---|---|---|---|
| $f_{geo}$ | 0.18 | 0.18 | 0.18 | 0.18 |
| $SC$ | 0.72 | 0.72 | 0.72 | 0.72 |
| $R_{inc}$ | 0.41 | 0.33 | 0.32 | 0.31 |
| $Y_{ref}$ | 0.72 | 0.56 | 0.78 | 1.1 |

These constants are used with the measured frequency profiles and ion current profiles to calculate the absolute sputtering yield using Eq. (1). The meanings of each of these are presented in the text.
$M = 0.11871$ kg/mol and $K = 2.79$E-26 kg/Hz for all cases.

## 3. Results and discussion

Over a wide range of temperatures and for two different ion species ($Ne^+$ and $Ar^+$), absolute sputtering yields were recorded. These data are shown in Fig. 3, and are presented as the ratio of the sputtering yield at the given temperature to that at room temperature (unheated) versus the ratio of the experimental temperature to tin's melting point (232 °C). The data show evidence of the suppression of temperature-enhanced sputtering yield measurements in comparison to previous results. Looking back to Fig. 1, we can see that the enhancement is more pronounced for the incident deuterium case than that for helium. Extending to heavier masses (see Fig. 3) shows even more suppressed enhancement for neon bombardment and no evidence for temperature enhancement outside of the error bars for $Ar^+$ bombardment for this particular range of temperatures. From this, we conclude that heavy-ion bombardment, while having a much larger sputtering yield, isn't as affected by surface temperature as that for light-ion bombardment. These results agree with previous examination of 8 keV heavy ion bombardment of silver, also showing very little temperature enhancement [16].

This is not to say that there is no temperature enhancement for heavy-ion bombardment above 350 °C. It is possible that the temperature at which temperature enhancement starts to play a significant role simply increases with increasing incident mass. This issue needs to be addressed before a definitive statement regarding the reduction of temperature-dependence of heavy-ion bombardment. However, the presence of temperature dependent sputtering properties for light-ion sputtering and the apparent suppression of it for heavy-ion bombardment is very intriguing.

Temperature-enhanced sputtering yields are not predictable using Sigmund's linear cascade theory [17,18], which claims direct proportionality between the energy deposited per unit depth and the sputtering yield. That is unless the energy deposition mechanisms are also temperature dependent. Therefore, if either the elastic

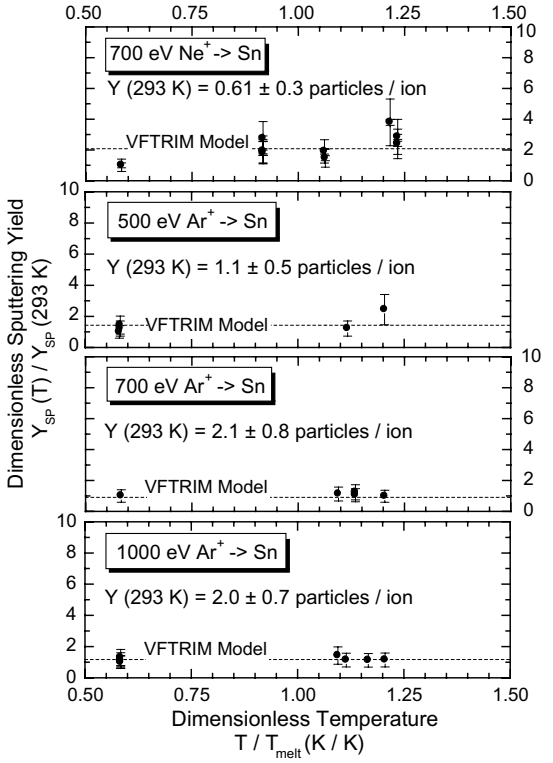


Fig. 3. These are the experimental results of this study for heavy-ion bombardment of tin at 45° incidence. Notice, especially in comparison to that seen for light ion irradiation, that there is little temperature enhancement of the sputtering yield. Also shown as a dashed horizontal line is the dimensionless sputtering yield found using the Monte Carlo atomistic simulation code VFTRIM [14].

(nuclear) or inelastic (electronic or phonon) losses can be shown to have temperature dependence for light-ion bombardment, but not for heavy, perhaps linear cascade theory can hold.

## 4. Conclusions

The effect of using increasingly heavy ions to irradiate a surface is the attenuation of the sputtering yields' temperature enhancement; while the absolute sputtering yield is much greater for heavy ions, as expected, the further increase as the sample is heated is diminished in comparison to the light-ion case. If the attenuation applies to even higher temperatures and heavier masses, this may indicate that tin self-sputtering would remain finite (with the redeposited tin flux equaling or exceeding the sputtering rate) as that previously modeled [1] with WBC [19] using solid tin self-sputtering yield simulation estimates. New efforts will focus on more heavy-ion work at higher target temperatures and lower ion energies to advance our collective understanding of both the behavior of a liquid tin surface under plasma bombardment and the physical processes behind the temperature enhancement.

## Acknowledgments

The authors would like to acknowledge and thank Ning Li for performing surface analysis on the QCM crystals; Eduardo Bringa, Jean-Paul Allain, and Bob Bastasz for helpful discussions; and Matt Hendricks, Dan Rokusek, Donna Carpenter, and Carolyn Tomchik for laboratory and data analysis assistance. This research is supported by DOE contract: DEFG 0299ER54515.

## References

[1] J.N. Brooks, Fus. Eng. Des. 60 (2002) 515.
[2] R.P. Doerner, M.J. Baldwin, et al., J. Nucl. Mater. 290–293 (2001) 166.
[3] M.J. Baldwin, R.P. Doerner, et al., Fus. Eng. Des. 61&62 (2002) 231.
[4] J.P. Allain, M.D. Coventry, D.N. Ruzic, J. Nucl. Mater. 313–316 (2003) 641.
[5] R.W. Conn, R.P. Doerner, et al., Nucl. Fusion 42 (2002) 1060.
[6] M.D. Coventry, J.P. Allain, D.N. Ruzic, J. Nucl. Mater. 335 (2004) 115.
[7] M.D. Coventry, J.P. Allain, D.N. Ruzic, J. Nucl. Mater. 313–316 (2003) 636.
[8] J.P. Allain, D.N. Ruzic, et al., Nucl. Instrum. and Meth. B, submitted for publication.
[9] R.P. Doerner, S.I. Krasheninnikov, K. Schmid, J. Appl. Phys. 95 (2004) 4471.
[10] R. Ranjan, J.P. Allain, et al., J. Vac. Sci. Technol. A 19 (2001) 1004.
[11] J.P. Allain, D.N. Ruzic, Nucl. Fusion 42 (2002) 202.
[12] M. Menzinger, L. Wahlin, Rev. Sci. Instrum. 40 (1969) 102.
[13] A. Fontell, E. Arminen, Can. J. Phys. 47 (1969) 2405.
[14] D.N. Ruzic, Nucl. Instrum. and Meth. B 47 (1990) 118.
[15] W. Eckstein, Computer Simulation of Ion–Solid Interactions, Springer Series in Materials Science, Berlin (1991).
[16] K. Besocke, S. Berger, et al., Radiat. Eff. 66 (1982) 35.
[17] P. Sigmund, Phys. Rev. 184 (1969) 383.
[18] P. Sigmund, Sputtering by Ion Bombardment: Theoretical Concepts, Sputtering by Particle Bombardment I, Berlin, 1981.
[19] J.N. Brooks, Phys. Fluids B 2 (1990) 1858.